Data reduction scheme for measuring G_{IIc} of wood in end-notched flexure (ENF) tests

Marcelo F.S.F. de Moura[1,*], Manuel A.L. Silva[2], José J.L. Morais[2], Alfredo B. de Morais[3] and José J.L. Lousada[2]

[1] Departamento de Engenharia Mecânica e Gestão Industrial, Faculdade de Engenharia, Universidade do Porto, Porto, Portugal

[2] CITAB – Centro de Investigação e de Tecnologias Agroambientais e Biológicas, Universidade de Trás-os-Montes e Alto Douro, Vila Real, Portugal

[3] Departamento de Engenharia Mecânica, Universidade de Aveiro, Campus Santiago, Aveiro, Portugal

*Corresponding author.
Departamento de Engenharia Mecânica e Gestão Industrial, Faculdade de Engenharia da Universidade do Porto, Rua Dr. Roberto Frias, 4200-465 Porto, Portugal
Phone: +351-22-5081727
Fax: +351-22-5081584
E-mail: mfmoura@fe.up.pt

Abstract

Numerical and experimental studies of end-notched flexure (ENF) fracture tests were performed to obtain mode II *R* curves for maritime pine (*Pinus pinaster* Ait.) wood in the radial-longitudinal (RL) crack propagation system. Three- (3D) and two-dimensional (2D) finite element analyses were conducted to determine the mode II release rate of the critical strain energy (G_{IIc}). The 3D analysis revealed that a small spurious mode III component did not affect G_{IIc} measurements and that the 2D model was very accurate. A new scheme for data reduction based on the equivalent crack concept is proposed to overcome the difficulties related to accurate crack length measurement during propagation. This method does not require previous experimental tests to obtain the elastic modulus, which varies markedly for different wood specimens. Experimental ENF tests were performed to verify the numerical results. The results demonstrate the accuracy of the data reduction method proposed.

Keywords: cohesive damage model; fracture characterization; mode II; wood.

Introduction

Wood is increasingly used in structural applications and interest in applying renewable resources in structures is also increasing for ecological reasons and because of energy shortages. However, these applications are still limited owing to a lack of failure criteria suited to the complex mechanical behavior of wood. Properties such as stiffness and strength are greatly influenced by the complex internal structure of wood. Macroscopically, wood can be considered an orthotropic material, with three local symmetry material directions: the longitudinal direction (L) is parallel to the axis of fibers or tracheids, the radial direction (R) is perpendicular to the growth rings, and the tangential direction (T) is perpendicular to the former. Thus, it is necessary to characterize six principal crack propagation systems, RL, TL, RT, LR, LT and TR, where the first letter represents the direction perpendicular to the crack plane and the second indicates the direction of crack propagation.

The RL crack propagation system was investigated in the present study. It is one of the most frequent crack propagation systems in timber beams (Smith and Vasic 2003) and bolted connections (Daudeville et al. 1999), and plays an important role in wood machining (Kopac and Sali 2003). It has been recognized that fracture mechanics provides a better description of failure than classical approaches that consider the material strength. Consequently, a fundamental requirement is to measure fracture properties such as the release rate of the critical strain energy in mode II. End-notched flexure (ENF) (Barrett and Foschi 1977; Yoshihara and Ohta, 2000; de Moura et al. 2006), end-loaded split (ELS) (Silva et al. 2007), and four-point end-notched flexure (4ENF) (Yoshihara 2004) tests were applied for wood fracture characterization in mode II. The ELS test involves a clamp, which is a source of variability and increases the complexity of data reduction (Blackman et al. 2005; Silva et al. 2007). On the other hand, the 4ENF test requires a more sophisticated set-up and specimens with a rectangular cross-section usually undergo bending failure before crack propagation. It was necessary to prepare specimens with an I-shaped cross-section to prevent bending failure and to induce mode II fracture (Yoshihara 2004). Consequently, the ENF configuration is the best for determining the mode II fracture properties of wood, mainly owing to its simplicity.

Nevertheless, there are some technical problems to be solved before the ENF can be accepted as a standard test for mode II fracture characterization of wood. The first is the difficulty associated with crack measurement throughout the test. In fact, in the ENF test, the crack tends to close during propagation, hindering clear identification of its tip. This can induce non-negligible errors in the derivative of the compliance relative to the crack length (dC/da) used in the compliance calibration method.

Moreover, wood as a natural material with considerable heterogeneity exhibits significant variation in Young's modulus between different specimens. This requires pre-measurement of the elastic properties before performing ENF tests. In the present study a new data reduction scheme for overcoming these difficulties is proposed. The method is based on the equivalent crack concept

and depends exclusively on specimen compliance. The method was first validated numerically and then applied to experimental data to obtain G_{IIc} values for *Pinus pinaster* wood samples.

Materials, methods and results

Cohesive damage model

The ENF specimen (Figure 1) had dimensions of $2h=20$ mm, $L=230$ mm, $L_1=250$ mm, $B=20$ mm and $a_0=162$ mm, which were chosen according to relations presented by Caumes (1987). Table 1 lists the nominal elastic and fracture properties of the maritime pine (*Pinus pinaster* Ait.) wood.

A cohesive mixed-mode damage model based on interface finite elements was considered to simulate damage onset and propagation. These elements were connected to solid elements to simulate the specimen arms and were placed at the mid-plane of the specimen where the pre-crack is located. A triangular constitutive relationship between stresses ($\boldsymbol{\sigma}$) and relative displacements ($\boldsymbol{\delta}$) at the interface was established (Figure 2). The subscripts "o" and "u" refer to onset and ultimate relative

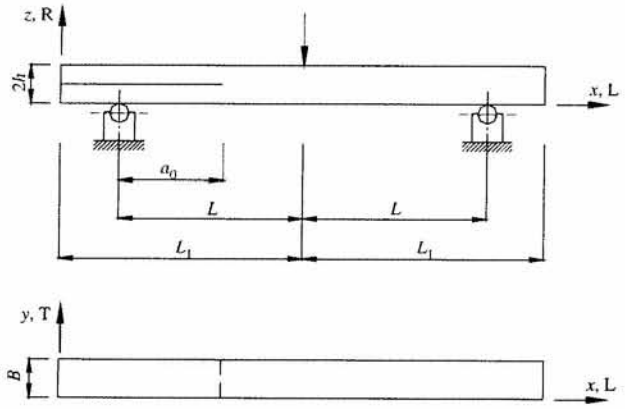

Figure 1 ENF specimen geometry.

Table 1 Nominal elastic and fracture properties of *Pinus pinaster* wood (de Moura et al. 2006).

Parameter	Value
E_L (GPa)	15.13
E_R (GPa)	1.91
E_T (GPa)	1.01
ν_{LR}	0.47
ν_{TL}	0.51
ν_{RT}	0.59
G_{LR} (GPa)	1.12
G_{LT} (GPa)	1.04
G_{RT} (GPa)	0.17
σ_L^{ult} (MPa)	97.46
σ_R^{ult} (MPa)	7.93
σ_T^{ult} (MPa)	4.20
τ_{RL}^{ult} (MPa)	16.0
τ_{LT}^{ult} (MPa)	16.0
τ_{RT}^{ult} (MPa)	4.54
G_{Ic} (N mm^{-1})	0.24
G_{IIc} (N mm^{-1})	0.63
G_{IIIc} (N mm^{-1})	0.90

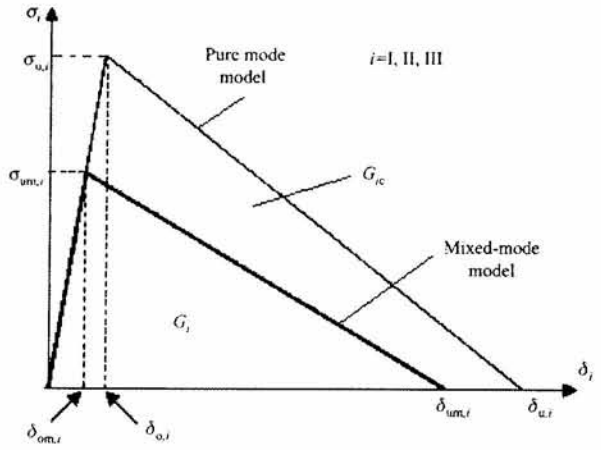

Figure 2 Pure- and mixed-mode damage model.

displacement, respectively, and the subscript "m" corresponds to the mixed mode. The model requires knowledge of the local strengths ($\sigma_{u,i}$, i=I, II, III) and the critical strain energy release rates (G_{ic}, i=I, II, III). The constitutive relationship before damage onset is:

$$\boldsymbol{\sigma}=\mathbf{E}\boldsymbol{\delta}_r, \tag{1}$$

where **E** is a diagonal stiffness matrix containing the stiffness parameter e. Its value must be quite high (10^6 N mm^{-3}) to avoid physically unacceptable interpenetrations. The softening relationship can be written as:

$$\boldsymbol{\sigma}=(\mathbf{I}-\mathbf{D})\mathbf{E}\boldsymbol{\delta}_r, \tag{2}$$

where **I** is the identity matrix and **D** is a diagonal matrix containing the damage parameter on the position corresponding to mode i (i=I, II, III). In general, structures are subjected to mixed-mode loading. Therefore, a formulation for interface finite elements should include a mixed-mode damage model (Figure 2). Damage onset was predicted based on a quadratic stress criterion:

$$\begin{aligned}&\left(\frac{\sigma_I}{\sigma_{u,I}}\right)^2+\left(\frac{\sigma_{II}}{\sigma_{u,II}}\right)^2+\left(\frac{\sigma_{III}}{\sigma_{u,III}}\right)^2=1 \quad \text{if} \quad \sigma_I>0\\ &\left(\frac{\sigma_{II}}{\sigma_{u,II}}\right)^2+\left(\frac{\sigma_{III}}{\sigma_{u,III}}\right)^2=1 \qquad\quad \text{if} \quad \sigma_I\le 0,\end{aligned} \tag{3}$$

where σ_i (i=I, II, III) represents the stress in each mode. Considering Eq. (1), the first equation in (3) can be rewritten as a function of the relative displacements:

$$\left(\frac{\delta_{om,I}}{\delta_{o,I}}\right)^2+\left(\frac{\delta_{om,II}}{\delta_{o,II}}\right)^2+\left(\frac{\delta_{om,III}}{\delta_{o,III}}\right)^2=1, \tag{4}$$

where $\delta_{om,i}$ (i=I, II, III) is the relative displacement corresponding to damage initiation in each mode. Crack propagation was simulated by the linear energetic criterion:

$$\frac{G_I}{G_{Ic}}+\frac{G_{II}}{G_{IIc}}+\frac{G_{III}}{G_{IIIc}}=1. \tag{5}$$

The area under the minor triangle of Figure 2 represents the energy released in each mode, whereas the area of the bigger triangle corresponds to the critical fracture energy. When Eq. (5) is satisfied, damage propagation occurs and stresses are completely released, with the exception of normal compressive stress. Based on the proposed criteria [(Eqs. (3 and 5)], it is possible to define the equivalent mixed-mode displacements δ_{om} and δ_{um}, thus establishing the damage parameters in the softening region:

$$d_m = \frac{\delta_{um}\,(\delta_m - \delta_{om})}{\delta_m\,(\delta_{um} - \delta_{om})}. \tag{6}$$

A detailed description of the model is presented by de Moura et al. (2006).

Data reduction schemes

Classical methods Normally, the G_{IIc} value is calculated from P-δ-a values by the compliance calibration method (CCM) or the corrected beam theory (CBT). The CCM is based on the Irwin-Kies equation (Kanninen and Popelar 1985):

$$G_{IIc} = \frac{P^2}{2B}\frac{dC}{da}, \tag{7}$$

where P represents the applied load, B the specimen width and $C = \delta/P$ the specimen compliance. Cubic polynomials ($C = C_1 a^3 + C_0$) are typically used to fit the $C = f(a)$ curves, which leads to:

$$G_{IIc} = \frac{3\,P^2 C_1\,a^2}{2B}. \tag{8}$$

In the case of ENF tests, Wang and Williams (1992) proposed the CBT:

$$G_{IIc} = \frac{9(a + 0.42\Delta_1)^2 P^2}{16B^2h^3E_1}, \tag{9}$$

where E_1 is the axial modulus, h is the half height of the specimen and Δ_1 is a crack length correction to account for shear deformation:

$$\Delta_1 = h\sqrt{\frac{E_1}{11G_{13}}\left[3\text{-}2\left(\frac{\Gamma}{1+\Gamma}\right)^2\right]} \tag{10}$$

with

$$\Gamma = 1.18\frac{\sqrt{E_1E_3}}{G_{13}}, \tag{11}$$

where E_3 and G_{13} are the transverse and shear moduli, respectively.

From Eqs. (8) and (9) it is evident that both of these methods require accurate crack length measurements during propagation, which are not easy to perform. In ENF fracture characterization tests, the crack tends to close due to the load applied, which hinders clear visualization of its tip. On the other hand, quite an extensive fracture process zone (FPZ) ahead of the crack tip occurs under mode II loading in wood. This non-negligible FPZ affects the fracture energy measured. Consequently, its influence should be taken into account, which does not occur when a real crack length is used in the selected data reduction scheme. To overcome these difficulties, a new data reduction scheme based on the crack equivalent concept and depending only on the specimen compliance was adopted in this study.

Compliance-based beam method As pointed out above, the aim of the present study was to apply CBBM for data reduction. The method is based on specimen compliance and on the equivalent crack concept. Based on beam theory including shear effects, the specimen compliance during crack propagation can be written as:

$$C = \frac{3a_{eq}^3 + 2L^3}{8E_fBh^3} + \frac{3L}{10G_{LR}Bh}, \tag{12}$$

where $a_{eq} = a + \Delta a_{FPZ}$ and Δa_{FPZ} is the crack length correction to account for the FPZ effect. Considering the initial crack length (a_0) and compliance (C_0), an estimate of the flexural modulus can be obtained from Eq. (12):

$$E_f = \frac{3a_0^3 + 2L^3}{8\,Bh^3C_{0corr}}, \tag{13}$$

where $C_{0\,corr}$ is given by:

$$C_{0\,corr} = C_0 - \frac{3L}{10G_{LR}Bh}. \tag{14}$$

During propagation, the equivalent crack length can be obtained from Eqs. (12) and (13):

$$a_{eq} = \left[\frac{C_{corr}}{C_{0\,corr}}a_0^3 + \frac{2}{3}\left(\frac{C_{corr}}{C_{0\,corr}} - 1\right)L^3\right]^{1/3}, \tag{15}$$

where C_{corr} is obtained from Eq. (14) with the current compliance C instead of C_0. Combining the Irwin-Kies equation (7) with Eq. (12) yields:

$$G_{IIc} = \frac{9P^2a_{eq}^2}{16B^2E_fh^3}, \tag{16}$$

where a_{eq} and E_f are given by Eqs. (15) and (13), respectively. This data reduction method does not require crack length measurement during tests, since a_{eq} is calculated from the specimen compliance. On the other hand, the flexural modulus is evaluated from the initial compliance experimentally measured. Consequently, the scheme does not require measurement of the flexural modulus in a separate test. Although G_{IIc} still depends on G_{LR}, it was verified that this parameter does not significantly influence the measured value of G_{IIc} (de Moura et al. 2006). The proposed method also accounts for energy dissipated in the non-negligible FPZ, as this material-weakening process influences specimen compliance.

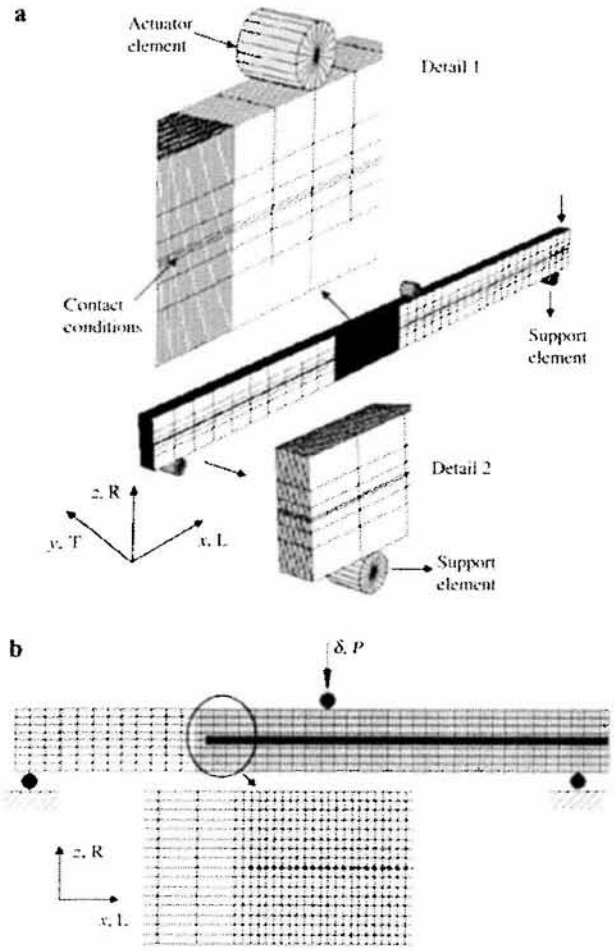

Figure 3 Mesh used in (a) the three-dimensional and (b) the two-dimensional finite element model.

Numerical analysis

Initially, we performed a three-dimensional (3D) finite element analysis (Figure 3a) using 3D eight-node brick elements from ABAQUS® software and previously developed eight-node interface finite elements (de Moura et al. 1997; Gonçalves et al. 2000). The finite element mesh has 30,250 brick elements and 4300 interface finite elements. The interface finite elements were placed at the mid-plane of the uncracked region (detail 1 in Figure 3a). Contact conditions were imposed in the region corresponding to the initial crack to avoid interpenetration of the specimen arms. Contact conditions were also imposed to simulate interaction between the actuator/supports and the ENF specimen (see details 1 and 2 in Figure 3a). The distributions of strain energy release rates (G_I, G_{II} and G_{III}) were obtained at the crack tip and along the specimen width by the virtual crack closure technique (Rybicki and Kanninen 1977). For the ENF specimen geometry considered, it was found that the average mode II component (G_{II}) was >99.8% of the total strain energy ($G_T = G_I + G_{II} + G_{III}$) (Figure 4).

A two-dimensional (2D) model was also considered to reduce the long computation time of the 3D model (Figure 3b). The specimen arms were modeled with 2750 plane strain eight-node quadrilateral solid finite elements (CPE8 from the ABAQUS® library) and 122 six-node

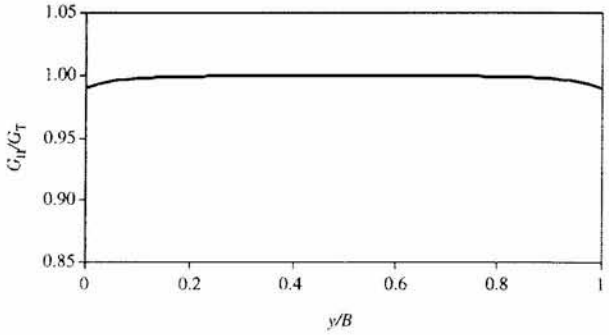

Figure 4 Distribution of G_{II}, normalized by the total strain energy (G_T), along the normalized width coordinate (y/B) of an ENF specimen.

interface elements were used to implement the cohesive damage model. Eight solid finite elements were applied through the thickness in each arm. In the damage propagation region a more refined mesh was used. Contact conditions were considered in the pre-crack region to avoid interpenetration of the specimen arms.

Crack growth simulation considering the 3D and 2D approaches was performed based on the proposed cohesive damage model. Small increments guaranteed a smooth propagation process. The numerical 3D and 2D load-displacement curves were in good agreement (Figure 5). G_{IIc} values were calculated by CCM [Eqs. (7) and (8)] with numerical values of P-δ-a. The performance of the 3D and 2D analyses was evaluated by comparison with the input G_{IIc} value. It was verified that both analyses could capture the value of G_{IIc} introduced (Figure 6), which demonstrates the suitability of the proposed model and of the 2D analysis.

Experimental tests

Maritime pine wood specimens were machined and tested. The material was conditioned at 20°C and 65% relative humidity until equilibrium was reached, which yielded a 12% moisture content in the wood. The average specific density was 0.55. The real dimensions were recorded for each of 24 specimens. The starter crack was introduced in two steps, just before the fracture test. Initially, a starter notch was machined with a band saw (1 mm in thickness). Then the crack was extended to 2–5 mm by applying a low-impact load on a cutting blade. The initial crack length, which is a fundamental parameter of the CBBM, was accurately measured on

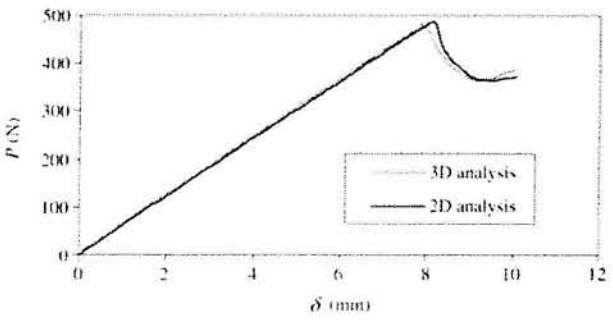

Figure 5 Comparison of numerical P-δ curves obtained from 2D and 3D approaches.

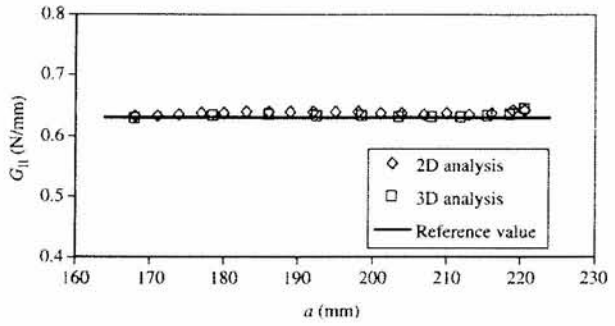

Figure 6 Comparison of apparent and input G_{IIc} values. The straight line corresponds to the input value of G_{IIc}.

both sides of the specimen to verify alignment of the crack front. Two sheets of Teflon film were inserted between the initial crack surfaces to minimize friction effects (Figure 7a). The mechanical tests were conducted in a screw-driven universal testing machine (Instron 1125). The specimen was supported by two cylinders and loaded at the mid-span at a crosshead speed of 5 mm min^{-1}. The applied load and displacement values were recorded (frequency 5 Hz) during fracture tests.

To measure the crack length during propagation, a scale was marked at one of the specimen edges. However, it was promptly concluded that important errors were being committed owing to dubious identification of the crack tip. In Figure 7b a discontinuity can be observed on the second black vertical reference line (detail 2). However, the crack tip position could not be defined, as virtually no changes are evident in the neighboring material. Moreover, it cannot be guaranteed that this discontinuity on the black line corresponds to a clear crack. Owing to quite extensive FPZ observed in mode

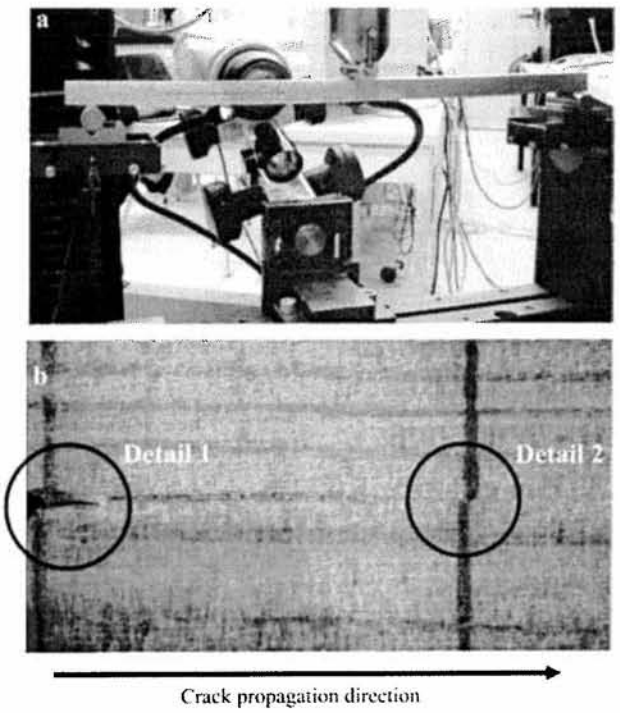

Figure 7 (a) Experimental set-up for ENF tests. (b) Microscope image of a crack during propagation: 1, initial crack tip; 2, undefined crack tip.

II fracture of wood, it can only be evidence of the softening process at the crack tip. In summary, it can be concluded that conventional data reduction schemes based on crack length measurements can lead to remarkable errors in G_{IIc} values.

Estimations of experimental initiation and critical values of G_{II} were obtained by applying the proposed CBBM. Figure 8a,b presents P-δ and R curves for all specimens tested. The R curves were obtained from the experimental P-δ curves by applying the CBBM, i.e., using Eqs. (13)–(16). In fact, from the current and initial compliance, the flexural modulus and equivalent crack length were calculated [Eqs. (13) and (15), respectively] and subsequently used to obtain G_{IIc}. Considerable scatter in initial specimen stiffness can be observed in Figure 8a, which reveals high modulus variability between different specimens. It should be emphasized that all samples were matched specimens cut from the same trunk.

Figure 9 shows the different fracture surfaces observed by SEM (Philips-FEI Quanta 400). Photomicrographs of the initial crack surface reveal three different zones. Figure 9a shows the typical pre-crack surface initiated by the saw and adjusted by a blade in mode I. The mode I fracture surface created ahead of the cutting blade exhibits the characteristic appearance of a fracture in perpendicular-to-grain tension through the middle lamella of tracheids (Zink et al. 1994). The transition between the pre-crack and mode II propagation surfaces is clearly visible in Figure 9b. Figure 9c shows in detail the typical fracture surfaces of mode II propagation, which are characterized by severe twisting, tearing, and unwinding of tracheid walls (Zink et al. 1994).

Discussion

To verify the performance of the CBBM, numerical simulations were performed based on the proposed cohe-

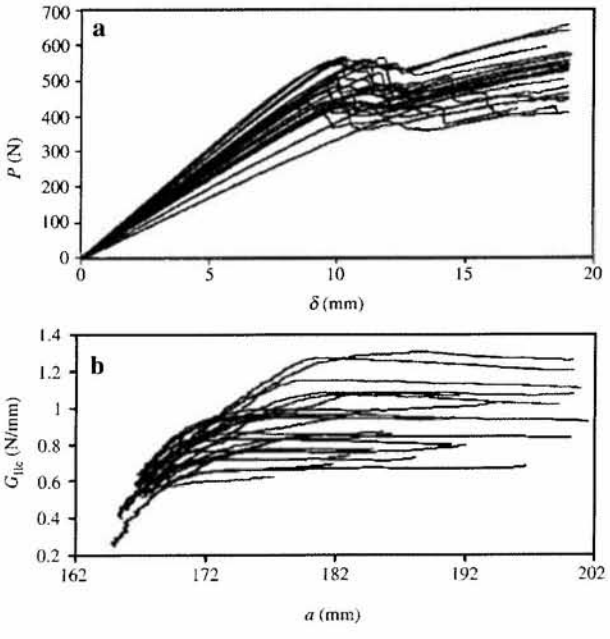

Figure 8 Experimental (a) P-δ and (b) R curves.

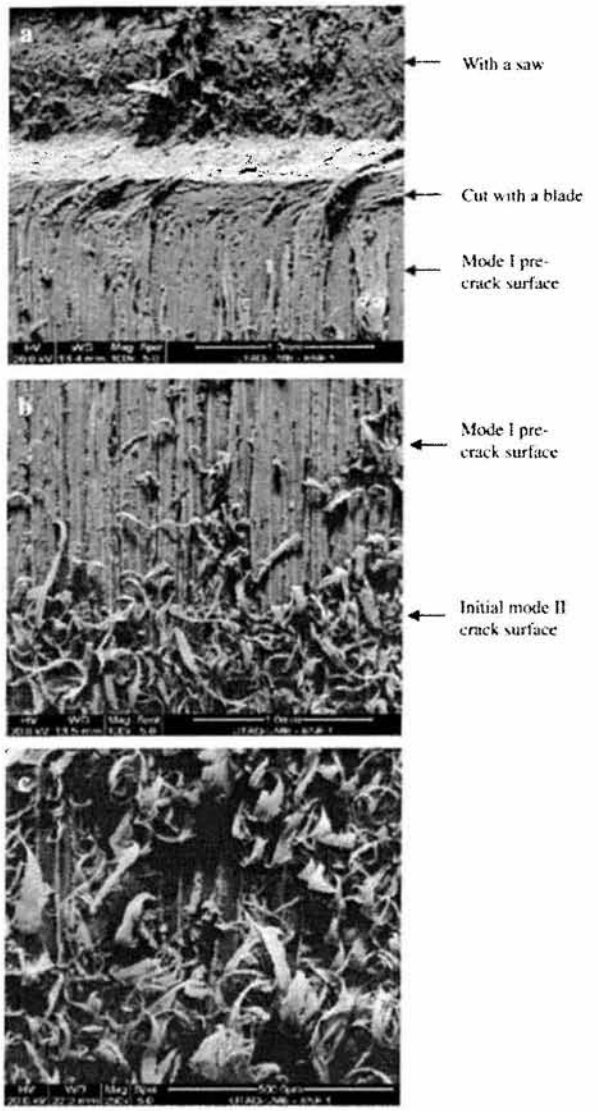

Figure 9 SEM micrographs: (a) pre-crack fracture surface; (b) transition between pre-crack and mode II fracture surfaces; and (c) detailed mode II fracture surface.

sive damage model for all specimens tested, and real parameters such as the elastic modulus and G_{IIc} were taken into consideration. The objective was to compare the numerical and experimental results for P-δ and R curves. Figure 10a,b illustrates typical experimental results. The initiation fracture energy $G_{II\,ini}$, corresponding to the initiation of FPZ development at the pre-crack tip, was taken at the onset of non-linearity of the P-δ curve. The G_{IIc} value, corresponding to self-similar stable crack propagation, was taken from the plateau of the R curve, and its value was input into the cohesive damage model.

Figure 11a exemplifies the good agreement obtained between numerical and experimental P-δ curves. This figure represents the best agreement obtained for specimen 10, but demonstrates that good agreement was generally achieved for the maximum load (Table 2). The mode II R curve considering the CBBM was obtained from the numerical P-δ results. Figure 11b shows the R curves corresponding to the P-δ curves of Figure 10. Good agreement in the plateau region is observed, which means that the experimental G_{IIc} value input in the cohesive damage model is well captured in the CBBM method. In addition, the R curve can be obtained by CBBM for a wide range of crack lengths when conducting ENF tests.

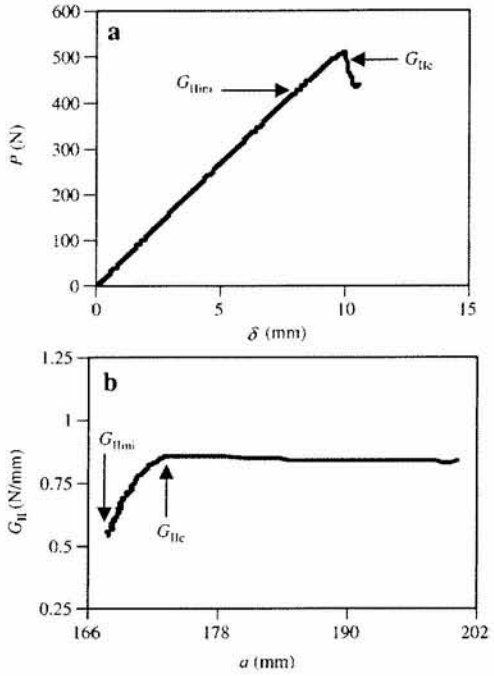

Figure 10 Typical experimental (a) P-δ and (b) R curves.

Table 2 summarizes the global results for all specimens. Standard deviation of approximately 20% was obtained for experimental G_{IIc} at the plateau, which can be considered as normal in wood. The average errors between numerical and experimental values for P_{max}, $G_{II\,ini}$ and G_{IIc} were less than 2%, which is excellent for wood. Therefore, the present study validates the CBBM for measuring the mode II fracture resistance of wood.

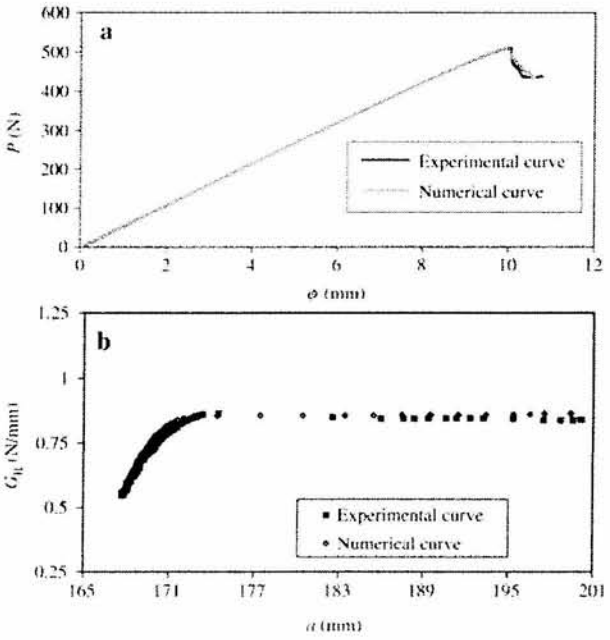

Figure 11 (a) Comparison of experimental and numerical (a) P-δ and (b) R curves for specimen 10.

Table 2 Summary of the experimental and numerical results for all specimens.

Specimen	Experimental results			Numerical results			Error		
	P_{max} (N)	$G_{II\,ini}$ (N mm^{-1})	G_{IIc} (N mm^{-1})	P_{max} (N)	$G_{II\,ini}$ (N mm^{-1})	G_{IIc} (N mm^{-1})	P_{max} (%)	$G_{II\,ini}$ (%)	G_{IIc} (%)
1	467.4	0.445	1.283	488.5	0.457	1.277	4.52	2.63	-0.50
2	507.5	0.398	1.269	528.4	0.396	1.264	4.11	-0.51	-0.33
3	564.4	0.635	1.139	579.4	0.635	1.143	2.67	0.05	0.44
4	469.2	0.579	0.772	475.7	0.573	0.762	1.39	-1.03	-1.22
5	414.4	0.252	0.667	416.3	0.257	0.649	0.48	1.98	-2.64
6	441.4	0.514	0.721	442.3	0.520	0.715	0.22	1.05	-0.84
7	549.5	0.573	0.994	579.4	0.580	0.967	5.44	1.16	-2.79
8	493.7	0.612	1.077	518.1	0.612	1.078	4.95	-0.12	0.14
9	510.8	0.545	0.845	510.3	0.547	0.858	-0.11	0.24	1.52
10	463.6	0.604	0.816	464.2	0.612	0.821	0.13	1.23	0.64
11	483.5	0.524	0.840	492.9	0.528	0.817	1.96	0.78	-2.67
12	423.0	0.537	0.601	425.7	0.537	0.590	0.63	0.01	-1.80
13	536.2	0.618	0.955	536.3	0.619	0.941	0.02	0.14	-1.44
14	521.6	0.550	1.060	536.8	0.552	1.052	2.90	0.43	-0.74
15	438.4	0.535	0.665	440.0	0.539	0.649	0.38	0.73	-2.40
16	567.7	0.740	0.992	566.6	0.742	0.980	-0.20	0.27	-1.21
17	441.0	0.516	0.845	459.3	0.517	0.833	3.93	0.05	-1.39
18	480.8	0.682	0.960	489.6	0.681	0.956	1.82	-0.15	-0.40
19	556.6	0.688	0.946	552.4	0.696	0.936	-0.74	1.16	-1.02
20	474.6	0.685	0.767	472.2	0.686	0.759	-0.50	0.19	-1.06
21	442.9	0.552	0.721	441.1	0.557	0.708	-0.41	1.00	-1.71
22	558.8	0.713	0.934	562.6	0.718	0.922	0.68	0.77	-1.36
23	559.3	0.649	1.085	576.5	0.652	1.075	3.08	0.46	-0.87
24	493.6	0.575	0.854	510.3	0.565	0.833	3.39	-1.58	-2.50
Mean	494.2	0.57	0.91	502.7	0.57	0.90	1.86[a]	0.74[a]	1.32[a]
CI	±19.44	±0.04	±0.07	±20.59	±0.04	±0.07			
SD (%)	9.83	18.71	20.16	10.24	18.57	20.63			

CI, 95% confidence interval; SD, standard deviation.
[a] Mean of absolute values.

The average experimental of G_{Ic}=0.91 N mm^{-1} is in agreement with the value of 0.93 N mm^{-1} measured in ELS tests for the same wood species (Silva et al. 2007). On the other hand, taking into account the complexities associated with clamping conditions in ELS tests, this result indicates that the ENF test is the most efficient method for characterizing wood by mode II fracture.

Conclusions

A new data reduction scheme is proposed based on the equivalent crack concept, which depends exclusively on specimen compliance, for ENF tests. The CBBM proposed does not depend on crack length monitoring during experimental tests and does not require additional experiments to obtain the elastic properties. Moreover, damage processes that weaken the material in the non-negligible FPZ dissipate an energy amount that should not be neglected for wood. All such mechanisms of energy dissipation in the FPZ influence the profile of the P-δ curve. Consequently, the equivalent crack length estimated from specimen compliance also includes the effect of these phenomena. In addition, the method provides access to the ENF R curve for a wide range of crack lengths when conducting the test.

Experiments verified that rigorous monitoring of crack length is very difficult and thus remarkable errors can be expected. This reinforced the advantages of the method proposed for data reduction. Initially, the CBBM was applied to results for ENF experimental load-displacement to obtain R curves. An experimental G_{IIc} value was input in the cohesive model. The numerical G_{IIc} value was estimated based on the numerical P-δ results. In general, good agreement was obtained between the numerical and experimental results for all specimens. Accordingly, CBBM represents a possible data reduction scheme for obtaining G_{IIc} values for wood. The method is very simple to apply, as it depends only on the experimental P-δ curve.

It was also observed that ENF and ELS tests provide similar values for G_{IIc}, but the ENF test is simpler to perform than the ELS. Consequently, the use of ENF tests in combination with the CBBM is the most appealing solution for standardized characterization of wood by mode II fracture.

Acknowledgements

The authors thank the Portuguese Foundation for Science and Technology for supporting this work through research project POCI/EME/56567/2004.

References

Barrett, J.D., Foschi, R.O. (1977) Mode II stress-intensity factors for cracked wood beams. Eng. Fract. Mech. 9:371–378.
Blackman, B.R.K., Kinloch, A.J., Paraschi, M. (2005) The deter-

mination of the mode II adhesive fracture resistance, G_{IIc}, of structural adhesive joints: an effective crack length approach. Eng. Fract. Mech. 72:877–897.

Caumes, P. (1987) Rupture d'un matériau anisotropic en conditions polymodales (Le bois). PhD thesis, Université de Bordeaux I, France.

Daudeville, L., Davenne, L., Yasumura, M. (1999) Prediction of load carrying capacity of bolted timber joints. Wood Sci. Technol. 33:15–29.

de Moura, M.F.S.F., Gonçalves, J.P.M., Marques, A.T., de Castro, P.M.S.T. (1997) Modelling compression failure after low velocity impact on laminated composites using interface elements. J. Compos. Mater. 31:1462–1479.

de Moura, M.F.S.F., Silva, M.A.L., de Morais, A.B., Morais, J.J.L. (2006) Equivalent crack based mode II fracture characterization of wood. Eng. Fract. Mech. 73:978–993.

Gonçalves, J.P., de Moura, M.F.S.F., de Castro P.M.S.T., Marques, A.T. (2000) Interface element including point-to-surface constraints for three dimensional problems with damage propagation. Eng. Comp. 17:28–47.

Kanninen, M.F., Popelar, C.H. Advanced Fracture Mechanics. Oxford University Press, 1985.

Kopac, J., Sali, S. (2003) Wood: an important material in manufacturing technology. J. Mater. Process. Technol. 133:134–142.

Rybicki, E.F., Kanninen, M.F. (1977) A finite element calculation of stress intensity factors by a modified crack closure integral. Eng. Fract. Mech. 9:931–938.

Silva, M.A.L., Morais, J.J.L., de Moura, M.F.S.F., Lousada, J.L. (2007) Mode II wood fracture characterization using the ELS test, Eng. Fract. Mech. 74:2133–2147.

Smith, I., Vasic, S. (2003) Fracture behavior of softwood. Mech. Mater. 35:803–815.

Yoshihara, H., Ohta, M. (2000) Measurement of mode II fracture toughness of wood by the end-notched flexure test. J. Wood Sci. 46:273–278.

Yoshihara, H. (2004) Mode II R-curve of wood measured by 4-ENF test. Eng. Fract. Mech. 71:2065–2077.

Wang, Y., Williams, J.G. (1992) Corrections for mode II fracture toughness specimens of composite materials. Compos. Sci. Technol. 43:251–256.

Zink, A.G., Pellicane, J., Shuler, C.E. (1994) Ultrastructural analysis of softwood fracture surfaces. Wood Sci. Technol. 28: 329–338.